Microchimica Acta (2020) 187: 464
https://doi.org/10.1007/s00604-020-04435-z

ORIGINAL PAPER

Determination of nereistoxin-related insecticide via quantum-dots-doped covalent organic frameworks in a molecularly imprinted network

Ying Zhang[1] · Xinyue Yuan[1] · Wei Jiang[1] · Huilin Liu[1]

Received: 29 March 2020 / Accepted: 7 July 2020 / Published online: 20 July 2020

Abstract

Quantum-dots-doped covalent organic frameworks in a molecularly imprinted network (QDs-doped COFs@MIP) were developed for detection of nereistoxin (NRT)-related insecticide in tap water. The preparation of QDs-doped COFs@MIP was easy to accomplish via one-pot synthesis at room temperature. QDs-doped COFs@MIP quenched by targeting thiosultap due to the photoinduced charge transfer. A Brunauer–Emmett–Teller surface area of 186.20 $m^2\ g^{-1}$ and a maximum adsorption capacity of 771 mg g^{-1} of the QDs-doped COFs@MIP exhibited good selectivity and adsorption capacity. Direct fluorescence determination was established over the range 5–100 μg L^{-1} ($R^2 = 0.9959$) with a detection limit of 1.60 μg L^{-1}. Furthermore, 86.5–106.5% recoveries of spiked tap water were achieved. The determination system was feasible for tracing the NRT-related insecticide with high accuracy and good repeatability and reproducibility.

Keywords Two modalities determination · Molecularly imprinted polymers · Covalent organic frameworks · Quantum dots · Nereistoxin-related insecticide

Introduction

Nereistoxin (NRT)-related insecticides, including thiosultap, cartap, thiocyclam, bensultap, and monosultap, were widely applied in agriculture pest management due to its low toxicity and high insecticidal activity [1]. Unfortunately, the overuse and/or misuse of NRT-related insecticides has caused food safety and environmental issues, and human health concerns [2, 3]. The Chinese Ministry of Agriculture has specified maximum residue limits (MRL) for NRT-related insecticide residues, such as the MRL of thiosultap in cabbage which is 0.5 mg kg^{-1}. The common methods for NRT-related insecticide detection are mainly instrumental analysis such as liquid chromatography/mass spectrometry [4, 5] and gas chromatography/mass spectrometry [6, 7] as they are high in sensitivity and accuracy. However, the inevitable shortcomings inherent in instrumental analysis such as its cost, complicated pretreatment steps, in-laboratory analysis, and skilled manpower limit their further application [8]. Therefore, a simple, environmentally friendly, low-cost, and convenient method for NRT-related insecticide identification at trace levels is particularly important.

Recently, the advancement in opto-sensors based on fluorescent quantum dots (QDs) has provided opportunity for convenient detection of chemical contaminants [9]. Mn–ZnS QDs are one of the most promising for applications because ZnS has a 3.7-eV-wide band gap [10] and has low toxicity. It has been extensively used as signal sources for metal-ion detection, biopolymers [10], and small molecules. However, bare-single Mn–ZnS QDs that are directly exposed to a complex matrix cannot detect analytes selectively and accurately. Molecular imprinting with high selectivity can make up for this defect, which combines with Mn–ZnS QDs to mimic the interaction in antibody–antigen systems to recognize target molecules [11, 12]. Three-dimensional imprinted cavities left by the removal of target molecules following polymerization

Electronic supplementary material The online version of this article (https://doi.org/10.1007/s00604-020-04435-z) contains supplementary material, which is available to authorized users.

✉ Huilin Liu
liuhuilin@btbu.edu.cn

[1] Beijing Advanced Innovation Center for Food Nutrition and Human Health, Beijing Engineering and Technology Research Center of Food Additives, Beijing Technology and Business University (BTBU), No. 11 Fucheng Road, Beijing 100048, People's Republic of China

enable superior selectivity. Molecularly imprinted polymers (MIPs) based on Mn–ZnS QDs were reported by many researchers, which combined the advantages of high selectivity of MIPs and good sensitivity of QDs to decrease detection limits [13–15]. However, the uniformity and response of QDs in MIPs are important indexes to improve the optosensing detection performance.

A further investigation of using covalent organic frameworks (COFs) as the support to prepare MIPs probe is of good distribution and performance for QDs [16–18]. COFs are extended porous crystalline and polymeric materials composed of light elements (C, N, O, and B) via reticular synthesis, and are held together by strong covalent bonds from discrete molecules [19–21]. The tailored synthesis and functionalization of COFs enable properties such as gas transport, catalysis, enzymes support, and electronic devices. COFs have large surface areas, uniform pore sizes, and high thermal and chemical stability to make it a potential support element.

Here, QDs-doped covalent organic frameworks in a molecularly imprinted network (QDs-doped COFs@MIP) were prepared via a one-pot reverse-microemulsion synthesis. It was used as a probe for the high-sensitivity determination of NRT-related insecticide in tap water via fluorescence spectra. The determination modality of sediment fluorescence determination (SFLD) not only avoids the interferences from the background, instrumental restrictions, and experimental errors but also improves accuracy and sensitivity for trace detection of chemical contaminants. The SFLD established a satisfying linear relationship to determine the NRT-related insecticide with a high accuracy. In addition, the thermal stability, isothermal adsorption, dynamic adsorption, and selectivity, recyclability, repeatability, and reproducibility of the QDs-doped COFs@MIP were investigated. The nanoparticles worked as an independent testing unit, and the flower-like COFs enhanced thiosultap adsorption. This technology was suitable for the analysis of all NRT-related insecticides by using the molecular template, and thiosultap was chosen as the model analyte. Thiosultap is soluble in water which increased the risk of water contamination. Due to the requirement of daily intake of tap water to maintain the body water balance, a safe and reliable tap water supply is important. Herein, the modality of SFLD was established for the detection of thiosultap in tap water with high accuracy and sensitivity.

Experiment

Materials and reagents

Thiosultap, cartap, bensultap, thiocyclam, monosultap standards, manganese acetate tetrahydrate ($Mn(Ac)_2{\cdot}4H_2O$), and 3-mercaptopropionic acid (MPA) were purchased from Aladdin Reagent Co., Ltd. (Shanghai, China, https://www.aladdin-e.com/). *P*-Phenylenediamine (Pa), mesitylene, 3-aminopropyl triethoxysilane (APTES), tetraethyl orthosilicate (TEOS), and Triton X-100 were supplied by Macklin Biochemical Technology Co., Ltd. (Shanghai, China, https://macklin.company.lookchem.cn/). Sodium sulfide ($Na_2S{\cdot}9H_2O$), ammonia solution (25 wt.%), and cyclohexane were obtained from Fuchen Chemical Reagents Co., Ltd. (Tianjin, China, http://www.tjfch.com/). Zinc sulfate heptahydrate ($ZnSO_4{\cdot}7H_2O$) was obtained from Xilong Science Co., Ltd. (Shanghai, China, http://www.xlhg.com/). Dioxane was supplied by J&K Scientific Ltd. (Beijing, China, https://www.jkchemical.com/). 1,3,5-Triformylphloroglucinol (TP) was supplied by Strem Chemicals, Inc. (Massachusetts, USA, https://www.strem.com/index.php). A Water Pro water purification system (Labconco, Kansas, MO, USA, https://www.labconco.com/) supplied doubly deionized water (DDW, 18.2 MΩ cm).

Apparatus

The fluorescence response of QDs-doped COFs@MIP to thiosultap was recorded on a multifunctional microplate reader (BioTek Instruments, Inc., USA, https://www.biotek.com/) under identical conditions. The excitation wavelength was 360 nm for emission over the range 400–650 nm. UV–visible spectra of thiosultap were acquired on a Cary 100 UV–Vis (Agilent, USA, https://www.agilent.com/) over the scan range of 200–400 nm. Surface morphologies of QDs-doped COFs@MIP, COFs, and Mn–ZnS QDs were imaged with scanning electron microscopy (SEM; S-4800, Hitachi, Ltd., Japan, http://www.hitachi.com/) and transmission electron microscopy (TEM; JEM-2012, JEOL Ltd., Japan, http://www.jeol.co.kr/). Fourier-transform infrared spectra (FT-IR) over the range 4000–650 cm^{-1} were acquired with a Nicolet iS10 (Thermo Scientific, USA, https://www.thermofisher.com). Thermogravimetric analysis (TGA) between 50 and 950 °C was performed with a STA 449 F3 Jupiter DTA-TG (Netzsch, Germany, https://www.netzsch.com/zh/) at a heating rate of 10 °C min^{-1} in air. X-ray diffraction (XRD) patterns were obtained with a Rigaku D/max-2500 diffractometer (Rigaku, Japan, https://www1.rigaku.com/ja) using Cu-K radiation. Brunauer–Emmett–Teller (BET) specific surface areas were measured via nitrogen adsorption on an ASAP 2460 physical adsorber (Micromeritics, American, https://www.micromeritics.com/).

Synthesis of quantum dots (QDs) and covalent organic frameworks (COFs)

Mn–ZnS QDs were synthesized as reported previously, with minor modifications [22]. More specific details are available in Electronic Supplementary Material.

The protocol for the synthesis of highly acid- and base-stable crystalline COFs was based on that of Kandambeth et al [23]. In a 500-mL conical flask containing 3 mL of mesitylene/dioxane (*v*/*v*, 1:1) solvent, Schiff-base reactions were performed with 63 mg of TP coupled with 48 mg of Pa in the presence of 3 M acetic acid (0.5 mL) at 120 °C for 3 days under air-tight conditions via N_2 bubbling. Under acidic condition, TP containing the active aldehyde group formed a Schiff base with Pa containing amino groups. Dark-red powdered COFs were obtained after washing with acetone and drying in vacuum at 180 °C for 24 h.

Synthesis of QDs-doped COFs@MIP

A schematic of the QDs-doped COFs@MIP composite is depicted in Fig. 1. In brief, 1.8 mL of Triton X-100 was mixed with 7.5 mL of cyclohexane in a 25-mL round-bottom flask for 15 min at room temperature with vigorous magnetic stirring. Then, 10 mg of Mn–ZnS QDs, 1 mg of COFs, 75 μL of TEOS, and 100 μL of ammonia solution were added. After mixing for 30 min, 37.5 μL of APTES and 100 μL of a thiosultap aqueous solution were added. The round-bottom flask was sealed with thin foil and thoroughly stirred magnetically for 24 h. Acetone (10 mL) and DDW (10 mL) were added sequentially three times to terminate the reaction and purify the product. Because the thiosultap is soluble in water, DDW was selected as the eluent to remove the thiosultap from polymers. The product was washed with DDW and centrifuged at 6000×*g* for 3 min sequentially several times until there was no signal corresponding to thiosultap at 245 nm in the UV–vis spectrum. The final QDs-doped COFs@MIP product was obtained by drying in a vacuum oven at 50 °C for 4 h. A control non-imprinted polymer (QDs-doped COFs@NIP) was obtained by the same process without addition of thiosultap. The polymers were thoroughly ground in a quartz mortar and sieved with 200-mesh screens before use.

Two modalities determination with the integrated system

QDs-doped COFs@MIP (4 mg) in thiosultap standard solution (4 mL, DDW as solvent) established an integrated system (1 mg mL^{-1}), where the two modalities SUVD and SFLD determinations at the upper and lower layers of the incubation material were performed. Then 200 μL and 3 mL of mixture were added to a 96-well plate and a four-sided transparent quartz cell with a 1 cm path length, respectively. The fluorescence response intensity of lower layers and UV–vis absorbance of upper layers to different thiosultap concentrations were recorded. The same procedure was performed with the QDs-doped COFs@NIP control. For more details about SFLD, please see Electronic Supplementary Material.

Recyclability, repeatability, and reproducibility

Further investigation was performed by recyclability, repeatability, and reproducibility experiments to evaluate the reusability of QDs-doped COFs@MIP. More details are presented in Electronic Supplementary Material.

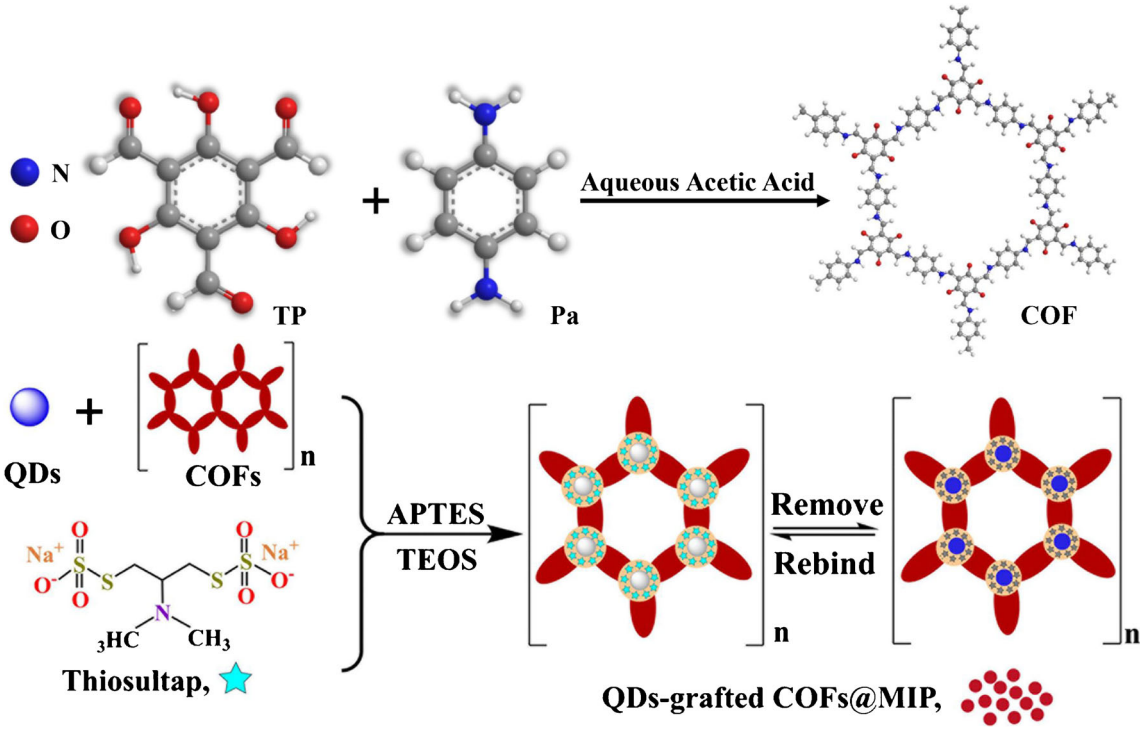

Fig. 1 Schematic of the composite of COF and QDs-doped COFs@MIP

Selectivity test

Selectivity test was conducted to assess the selectivity of the QDs-doped COFs@MIP. For more details, please see Electronic Supplementary Material.

Sample pretreatment

Tap water was collected and spiked with various amounts of thiosultap for final concentrations of 50, 70, and 90 μg L^{-1} for SFLD analysis. No pretreatment was carried out for the water sample.

Results and discussion

Preparation and detection mechanism of QDs-doped COFs@MIP

A schematic of the detection of residual thiosultap based on quantum-dots-doped covalent organic frameworks in a molecularly imprinted network is shown in Fig. 1. The surface of the Mn–ZnS QDs was coated with silica via the hydrolysis and condensation reactions of TEOS and APTES, and the amino was anchored on the Mn–ZnS QDs as an antenna. In the cross-linked polymer matrix, the strong hydrogen bonds between amino and thiosultap during imprinting process created selective thiosultap binding sites with the right shape and orientation after the removal of the thiosultap template.

The fluorescence of QDs-doped COFs@MIP quenched after selectively interacting with thiosultap. The UV absorption of thiosultap was far away from fluorescence emission spectrum of the QDs (Fig. 2a), so we conjectured that the photo-induced charge transfer is the most likely mechanism of fluorescence quenching instead of fluorescence resonance energy transfer. The frontier molecular orbital theory can be used to explain the quenching mechanism, as shown in Fig. 2b. The electrons of QDs migrated from valence band to conduction band under light excitation. The blue fluorescence was emitted from QDs when excited electrons returned to ground state. In the presence of thiosultap, QDs-doped COFs@MIP interacted with thiosultap via hydrogen bonds, resulting in charge transfer. The thiosultap UV–vis absorption band at 245 nm approached the Mn–ZnS QDs conduction band gap. This made it possible that excited electrons in the highest occupied molecular orbital (HOMO) jumped directly to the lowest unoccupied molecular orbital (LUMO) of thiosultap, which made the fluorescence quench.

The imprinting efficiency and affinity of QDs-doped COFs@MIP for thiosultap was dependent on the quantity of functional monomers. The molar ratio of template to APTES was also important because it determined the number of recognition sites. An evaluation and optimization of template–functional monomer–cross-linker molar ratios (1:300:600, 1:400:800, 1:600:1200, 1:800:1600) was performed. The imprinting factor (IF) was used to determine the optimal molar ratio with which the QDs-doped COFs@MIP had the highest adsorption capacity. Table 1 indicates that the highest adsorption capacity and the strongest molecular recognition were observed for a thiosultap–APTES–TEOS molar ratio of 1:600:1200.

Characterization

The morphologies of QDs-doped COFs@MIP, COFs, and Mn–ZnS QDs were characterized with SEM and TEM. In Fig. 3a, the black dots uniformly dispersed in the TEM image of Mn–ZnS QDs had 5-nm diameters. The SEM image of COFs in Fig. 3b revealed a multi-branched flowerlike morphology. The SEM image in Fig. 3c of QDs-doped

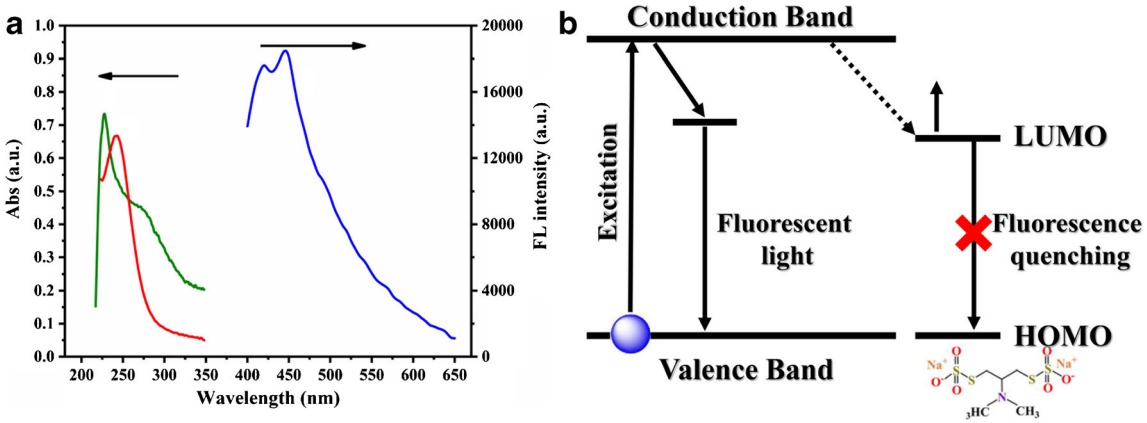

Fig. 2 (**a**) UV–vis spectra of Mn–ZnS QDs (green line) and thiosultap (red line, maximum absorption at 245 nm). Emission spectra (blue line) of Mn–ZnS QDs with emission wavelength of 450 nm at excitation wavelength of 360 nm. (**b**) Schematic of molecular orbital the theory for the fluorescence quenching mechanism

Table 1 Optimization of the molar ratio of thiosultap and APTES

Thiosultap	APTES	TEOS	$K_{SV,\ QDs\text{-}grafted\ COFs@MIP}$	$K_{SV,\ QDs\text{-}grafted\ COFs@NIP}$	IF
1	300	600	0.0091 ± 0.0001	0.0067 ± 0.0005	1.35 ± 0.02
1	400	800	0.0174 ± 0.0004		2.59 ± 0.06
1	600	1200	0.0342 ± 0.0004		4.59 ± 0.07
1	800	1600	0.0145 ± 0.0002		2.15 ± 0.03

COFs@MIP revealed a uniform, highly spherical morphology with 20–40-nm diameters and rough surfaces, which was consistent with the TEM image of QDs-doped COFs@MIP (Fig. 3d). Their BET surface areas were 186.2 $m^2\ g^{-1}$, which were much higher than those of NIP (45.4 $m^2\ g^{-1}$). The superior surface adsorption capacity of QDs-doped COFs@MIP reflected its uniform and nanoscale structure.

To further explore the positive effect of COF, more characterization by the combination of FT-IR, TGA, DTG, and XRD was conducted. The results are shown in Fig. S1. The results of equilibrium isotherms of thiosultap adsorption on QDs-doped COFs@MIP and QDs-doped COFs NIP are presented in Fig. S2. Also, the effect of shaking and incubation time on the fluorescence intensity and adsorption amounts were investigated. The results are shown in Fig. S3.

The determination of thiosultap

In SFLD, the fluorescence intensity decreased as the concentration of thiosultap increased (Fig. 4a). The QDs-doped COFs@MIP exhibited linear fluorescence quenching at the excitation/emission wavelength of 450 nm/360 nm versus thiosultap concentrations in the low range of 5–100 μg L^{-1}, where $F_0/F = 0.0342[C] + 0.905$, with $R^2 = 0.9959$ (Fig. 4b). For the control, R^2 for NIP was 0.7891, with $F_0/F = 0.0066[C] + 0.915$. The limit of detection (LOD) was calculated as 1.6 μg L^{-1} by using the formula $LOD = 3\sigma/Ksv$, where σ is the SD of tested blank with six repetitions. The low LOD of 1.6 μg L^{-1} satisfied the limited standard of GB 2763-2016.

Compared with SFLD, the indirect SUVD presented a linear relationship between absorbance at the

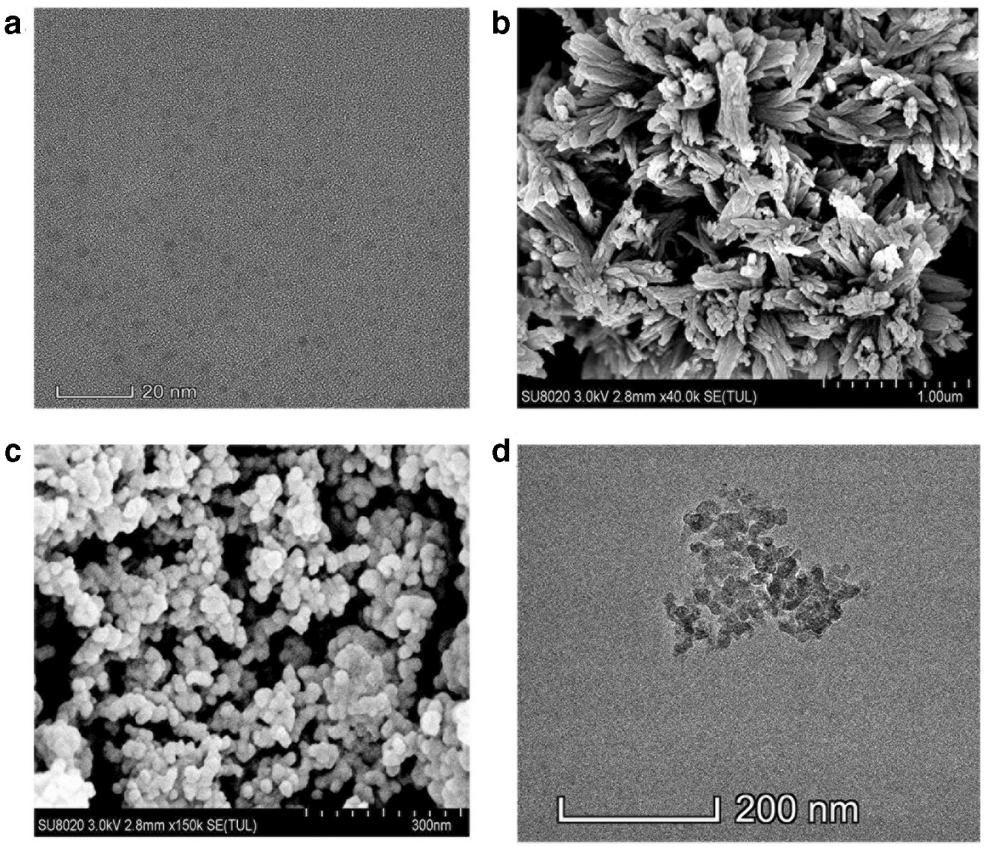

Fig. 3 (**a**) TEM images of Mn-ZnS QDs. (**b**) SEM images of COFs. (**c**) SEM images and (**d**) TEM image of QDs-doped COFs@MIP

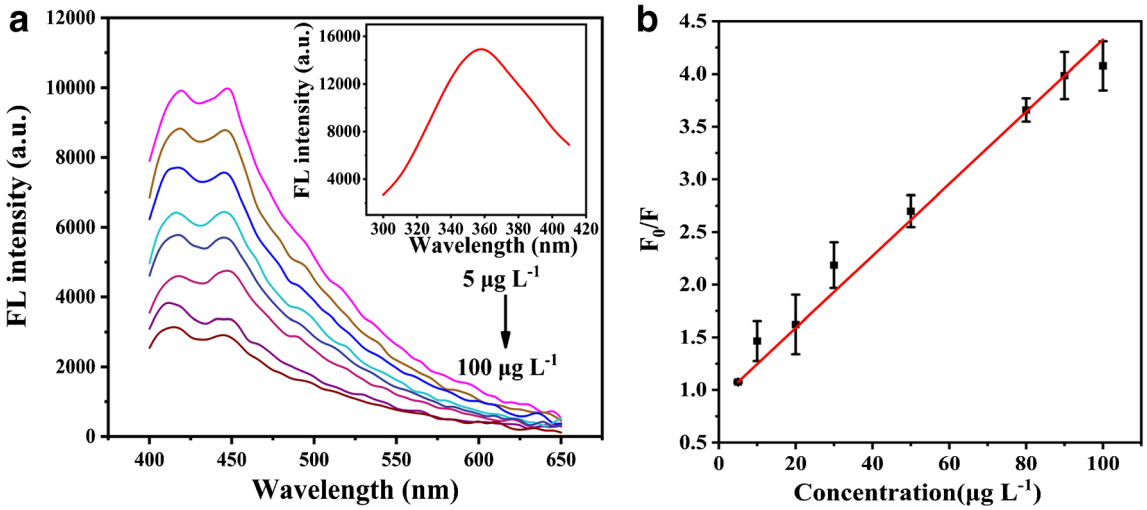

Fig. 4 (**a**) Fluorescence emission spectra of QDs-doped COFs@MIP with the addition of the indicated thiosultap concentrations ranging over 5–100 μg L^{-1} (inset—excitation spectra of QDs-doped COFs@MIP with a maximum at 360 nm). (**b**) The Stern–Volmer plot in SFLD

wavelength of 245 nm and thiosultap concentration over a high range of 200–2500 mg L^{-1} with a LOD of 31 mg L^{-1} (more details are shown in the Electronic Supplementary Material). Therefore, the direct SFLD and indirect SUVD had significant difference in the determination of thiosultap. The determination modality of SFLD had an even lower LOD of 1.6 μg L^{-1} and was selected for its superior sensitivity.

Recyclability, repeatability, and reproducibility

The recyclability, repeatability, and reproducibility of QDs-doped COFs@MIP were investigated, and the results are presented in Fig. S5.

Selective adsorption of thiosultap

Cartap, bensultap, thiocyclam, and monosultap were used as structural analogues (Fig. S6) to verify selective adsorption of thiosultap on QDs-doped COFs@MIP. Figure 5a (inset) shows that for SFLD, there were more significant fluorescence changes for thiosultap with increased concentration than for the structural analogues. The SF were 5.86, 5.78, 9.03, and 8.27 for monosultap, thiocyclam, bensultap, and cartap, respectively. Hence, QDs-doped COFs@MIP was very selective for thiosultap in shape, size, and spatial distribution due to the template sites. Furthermore, in Fig. 5b, the QIF of thiosultap were 19.66, whereas those of monosultap, thiocyclam, bensultap, and cartap were 3.24, 3.10, 2.33, and 2.62,

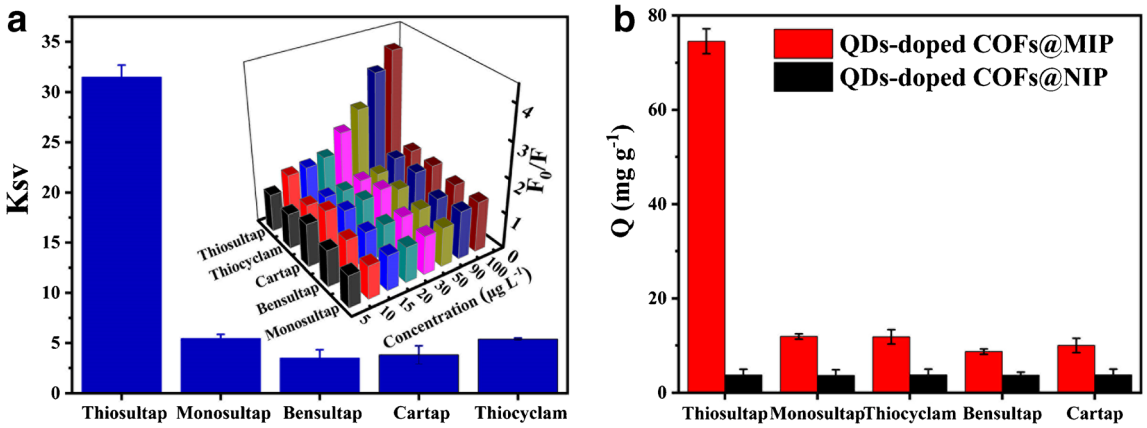

Fig. 5 (**a**) Quenching constant of QDs-doped COFs@MIP to thiosultap and structural analogues in SFLD (inset—fluorescence changes for thiosultap and structural analogues with increased concentrations). (**b**) Adsorption capacities for thiosultap and structural analogues on QDs-doped COFs@MIP and QDs-doped COFs@NIP in SUVD. (The concentrations of thiosultap and the structural analogues were 100 mg L^{-1})

Table 2 Recoveries of thiosultap for spiked samples ($n = 3$)

Method	Added ($\mu g\ L^{-1}$)	Found ($\mu g\ L^{-1}$)	Recovery (%)	RSD (%)
SFLD	0	–	–	–
	50	45.21	90.42	5.18
	70	60.57	86.53	4.24
	90	95.81	106.45	2.56

respectively. The QSF were 6.26, 6.30, 8.57, and 7.45, respectively, for the structural analogues. Thus, the imprinted QDs-doped COFs@MIP exhibited highly selective recognition for thiosultap.

Analysis of spiked samples

The ability to quantify a spiked thiosultap concentration in a real sample was examined, as shown in Table 2. No response corresponding to thiosultap in tap water was observed by SFLD. For three different spiked levels, 86.53–106.45% recoveries were obtained for SFLD with RSD values less than 5.36%, indicating an accredited accuracy for trace thiosultap detection. Furthermore, other literature reports concerning the nereistoxin-related insecticide detection are summarized in Table 3. Compared with other methods for the nereistoxin-related insecticide detection, the SFLD has low detection limit and exhibits high selectivity.

Conclusion

Optosensing detection of thiosultap based on a COF-supported MIP with a core of Mn–ZnS QDs was demonstrated. In particular, the direct sediment fluorescence determination was demonstrated and applied to the analysis of thiosultap in tap water with high precision and accuracy. However, the need for working in the UV makes the probe prone to

Table 3 An overview on recently reported nanomaterial-based optical methods for the determination of nereistoxin-related insecticide

Methods	Target	LOD	Linear range	Sample	Recovery (%)	Reference
Colorimetry using UV–vis spectroscopy based on direct using of AuNPs	Cartap	0.04 mg kg^{-1} (40 $\mu g\ L^{-1}$)	0.05–0.6 mg kg^{-1} (50–600 $\mu g\ L^{-1}$)	Cabbage, tea	71.8–104.0	[24]
The visual and colorimetric determination based on the unmodified AuNPs	Total nereistoxin-related insecticides	40 $\mu g\ kg^{-1}$ (40 $\mu g\ L^{-1}$)	50–250 $\mu g\ kg^{-1}$ (50–250 $\mu g\ L^{-1}$)	Tea, kiwifruit, rice, cabbage	61.0–105.0	[2]
LC-MS/MS method based on a reversed-phase C_8 column (150 mm × 4.6 mm × 5 μm)	Thiosultap sodium, thiocyclam, and nereistoxin	0.1 $\mu g\ kg^{-1}$ (0.1 $\mu g\ L^{-1}$)	0.001–0.5 mg/kg (1–500 $\mu g\ L^{-1}$)	Pepper	58.0–87.0	[5]
GC-FPD-S method based on a capillary column (Supelco equity-5, 30 m × 0.25 mm ID, 0.25 μm thickness film)	Monosultap	0.01 mg kg^{-1} (10 $\mu g\ L^{-1}$) (LOQ)	0.1–30 $\mu g\ mL^{-1}$ (100–30,000 $\mu g\ L^{-1}$)	Tomato, soil	86.5–101.7	[7]
Electrochemical sensing based on electron transfer promotion effect on an Au electrode	Cartap, bensultap	–	–	–	–	[25]
Colorimetric determination using UV–vis spectroscopy based on AuNPs	Thiocyclam, bensultap, cartap	12 ng mL^{-1} (12 $\mu g\ L^{-1}$)	12–140 ng mL^{-1} (12–140 $\mu g\ L^{-1}$)	Environmental water	94.0–106.0	[3]
HILIC-MS/MS method based on HILIC column (150 × 2.1 mm, 5 μm particle size)	Cartap and its metabolite	2 $\mu g\ kg^{-1}$ (2 $\mu g\ L^{-1}$)	0.5–100 $\mu g\ kg^{-1}$ (0.5–100 $\mu g\ L^{-1}$)	Tea	87.6–119.9	[26]
Colorimetric detection using UV–vis spectroscopy based on AgNP sensor	Cartap	0.01 mg L^{-1} (10 $\mu g\ L^{-1}$)	0.1–5 mg L^{-1} (100-5000 $\mu g\ L^{-1}$)	Tea beverages	98.3–101.6	[27]
Homogeneous electrochemical detection based on an ultramicroelectrode	Bensultap	6.9 ng L^{-1} (0.0069 $\mu g\ L^{-1}$)	0.01–2000 ng L^{-1} (0.00001–2 $\mu g\ L^{-1}$)	Cabbage, apple	86.8–95.3	[8]
Fluorometric determination based on green emitting carbon dots and AuNPs	Cartap	3.8 nM (0.9006 $\mu g\ L^{-1}$)	5–300 nM (1.185–71.1 $\mu g\ L^{-1}$)	Tap water, cabbage	99.2–101.7	[28]
Fluorescence sensing and UV spectroscopy based on QDs-doped COFs@MIP	Thiosultap	1.6 $\mu g\ L^{-1}$	5–100 $\mu g\ L^{-1}$ 200–2500 mg L^{-1}	Tap water	86.53–106.45	This paper

interferences by biomatter. The UV light used for fluorescence excitation will be screened off by UV absorbers and this will weaken the signal. This advanced sensing material was prepared in a one-pot synthesis and laid the foundation for applying the determination of thiosultap in complex food matrices.

Acknowledgments This work was supported by the National Key R&D Program of China (No. 2018YFC1602300), the National Natural Science Foundation of China (No. 31822040), the Young Top-Notch Talent of High-Level Innovation and Entrepreneurs Support Program (No. 2017000026833ZK28), and School Level Cultivation Fund of Beijing Technology and Business University for Distinguished and Excellent Young Scholars (BTBUYP2020).

Compliance with ethical standards

Conflict of interest The authors declare that they have no competing interests.

References

1. Liu W, Zhang D, Zhu W, Zhang S, Wang Y, Yu S, Liu T, Zhang X, Zhang W, Wang J (2015) Colorimetric and visual determination of total nereistoxin-related insecticides by exploiting a nereistoxin-driven aggregation of gold nanoparticles. Microchim Acta 182(1): 401–408. https://doi.org/10.1007/s00604-014-1347-x
2. Kurisaki E, Kato N, Ishida T, Matsumoto A, Shinohara K, Hiraiwa K (2010) Fatal human poisoning with Padan™: a cartap-containing pesticide. Clin Toxicol 48(2):153–155. https://doi.org/10.3109/15563650903505166
3. Takahashi F, Yamamoto N, Todoriki M, Jin J (2018) Sonochemical preparation of gold nanoparticles for sensitive colorimetric determination of nereistoxin insecticides in environmental samples. Talanta 188:651–657. https://doi.org/10.1016/j.talanta.2018.06.042
4. Ferrer C, Mezcua M, Martínez-Uroz MA, Pareja L, Lozano A, Fernández-Alba AR (2010) Method development and validation for determination of thiosultap sodium, thiocyclam, and nereistoxin in pepper matrix. Anal Bioanal Chem 398(5):2299–2306. https://doi.org/10.1007/s00216-010-4100-2
5. Wang Z, Wu L, Shen B, Jiang Z (2013) Highly sensitive and selective cartap nanosensor based on luminescence resonance energy transfer between $NaYF_4$:Yb,Ho nanocrystals and gold nanoparticles. Talanta 114:124–130. https://doi.org/10.1016/j.talanta.2013.02.069
6. Park Y, Choe S, Lee H, Jo J, Park Y, Kim E, Pyo J, Jung JH (2015) Advanced analytical method of nereistoxin using mixed-mode cationic exchange solid-phase extraction and GC/MS. Forensic Sci Int 252:143–149. https://doi.org/10.1016/j.forsciint.2015.04.010
7. Tao CJ, Hu JY, Li JZ (2007) Determination of insecticide monosultap residues in tomato and soil by capillary gas chromatography with flame photometric detection. Can J Anal Sci Spectrosc 52(5):295–304
8. Xie S, Yuan W, Wang P, Tang Y, Teng L, Peng Q (2019) Target-induced conformational switch of DNAzyme for homogeneous electrochemical detection of nereistoxin-related insecticide on an ultramicroelectrode. Sensors Actuators B Chem 292:64–69. https://doi.org/10.1016/j.snb.2019.04.095
9. Durán-Toro V, Gran-Scheuch A, Órdenes-Aenishanslins N, Monrás JP, Saona LA, Venegas FA, Chasteen TG, Bravo D, Pérez-Donoso JM (2014) Quantum dot-based assay for Cu^{2+} quantification in bacterial cell culture. Anal Biochem 450:30–36. https://doi.org/10.1016/j.ab.2014.01.001
10. Chang L, He X, Chen L, Zhang Y (2017) Mercaptophenylboronic acid-capped Mn-doped ZnS quantum dots for highly selective and sensitive fluorescence detection of glycoproteins. Sensors Actuators B Chem 243:72–77. https://doi.org/10.1016/j.snb.2016.11.121
11. Gómez-Arribas LN, Urraca JL, Benito-Peña E, Moreno-Bondi MC (2019) Tag-specific affinity purification of recombinant proteins by using molecularly imprinted polymers. Anal Chem 91(6):4100–4106. https://doi.org/10.1021/acs.analchem.8b05731
12. Guo J, Yu M, Wei X, Huang L (2018) Preparation of core–shell magnetic molecularly imprinted polymer with uniform thin polymer layer for adsorption of dichlorophen. J Chem Eng Data 63(8): 3068–3073. https://doi.org/10.1021/acs.jced.8b00321
13. Ren X, Chen L (2015) Quantum dots coated with molecularly imprinted polymer as fluorescence probe for detection of cyphenothrin. Biosens Bioelectron 64:182–188. https://doi.org/10.1016/j.bios.2014.08.086
14. Luo SQ, Miao YM, Guo JP, Sun XJ, Yan GQ (2019) Phosphorimetric determination of 4-nitrophenol using mesoporous molecular imprinting polymers containing manganese(II)-doped ZnS quantum dots. Microchim Acta 186(4):249. https://doi.org/10.1007/s00604-019-3362-4
15. Chen SJ, Li YZ, Wu SW, Jiang XL, Yang H, Su X, He L, Zou LK, Ao XL, Liu SL, Yang Y (2020) A phosphorescent probe for cephalexin consisting of mesoporous thioglycolic acid-modified Mn:ZnS quantum dots coated with a molecularly imprinted polymer. Microchim Acta 187(1):10. https://doi.org/10.1007/s00604-019-4038-9
16. Zhang D, Wang Y, Xie J, Geng W, Liu H (2020) Ionic-liquid-stabilized fluorescent probe based on S-doped carbon dot-embedded covalent-organic frameworks for determination of histamine. Microchim Acta 187:28. https://doi.org/10.1007/s00604-019-3833-7
17. Ni T, Zhang D, Wang J, Wang S, Liu H, Sun B (2018) Grafting of quantum dots on covalent organic frameworks via a reverse microemulsion for highly selective and sensitive protein optosensing. Sensors Actuators B 269:340–345. https://doi.org/10.1016/j.snb.2018.04.172
18. Liu H, Zhang Y, Zhang D, Zheng F, Huang M, Sun J, Sun X, Li H, Wang J, Sun B (2019) A fluorescent nanoprobe for 4-ethylguaiacol based on the use of a molecularly imprinted polymer doped with a covalent organic framework grafted onto carbon nanodots. Microchim Acta 186(3):182. https://doi.org/10.1007/s00604-019-3306-z
19. Zhang D, Liu H, Geng W, Wang Y (2019) A dual-function molecularly imprinted optopolymer based on quantum dots grafted covalent-organic frameworks for the sensitive detection of tyramine in fermented meat products. Food Chem 277:639–645. https://doi.org/10.1016/j.foodchem.2018.10.147
20. Côté AP, Benin AI, Ockwig NW, Keeffe M, Matzger AJ, Yaghi OM (2005) Porous, crystalline, covalent organic frameworks. Science 310(5751):1166–1170. https://doi.org/10.1126/science.1120411
21. Lewis GN (1916) The atom and the molecule. J Am Chem Soc 38(4):762–785. https://doi.org/10.1021/ja02261a002
22. Zhuang J, Zhang X, Wang G, Li D, Yang W, Li T (2003) Synthesis of water-soluble ZnS : Mn^{2+} nanocrystals by using mercaptopropionic acid as stabilizer. J Mater Chem 13(7):1853–1857. https://doi.org/10.1039/B303287F
23. Kandambeth S, Mallick A, Lukose B, Mane MV, Heine T, Banerjee R (2012) Construction of crystalline 2D covalent organic frameworks with remarkable chemical (acid/base) stability via a combined reversible and irreversible route. J Am Chem Soc 134(48):19524–19527. https://doi.org/10.1021/ja308278w

24. Liu W, Zhang D, Tang Y, Wang Y, Yan F, Li Z, Wang J, Zhou HS (2012) Highly sensitive and selective colorimetric detection of cartap residue in agricultural products. Talanta 101:382–387. https://doi.org/10.1016/j.talanta.2012.09.045
25. Shimada H, Noguchi S, Yamamoto M, Nishiyama K, Kitamura Y, Ihara T (2017) Electrochemical sensing of neurotoxic agents based on their electron transfer promotion effect on an Au electrode. Anal Chem 89(11):5742–5747. https://doi.org/10.1021/acs.analchem.6b04229
26. Dai J, Chen H, Gao G, Zhu L, Chai Y, Liu X (2019) Simultaneous determination of cartap and its metabolite in tea using hydrophilic interaction chromatography tandem mass spectrometry and the combination of dispersive solid phase extraction and solid phase extraction. J Chromatogr A 1600:148–157. https://doi.org/10.1016/j.chroma.2019.04.034
27. Wu M, Deng H, Fan Y, Hu Y, Guo Y, Xie L (2018) Rapid colorimetric detection of cartap residues by AgNP sensor with magnetic molecularly imprinted microspheres as recognition elements. Molecules 23(6). https://doi.org/10.3390/molecules23061443
28. Yang Y, Hou J, Huo D, Wang X, Li J, Xu G, Bian M, He Q, Hou C, Yang M (2019) Green emitting carbon dots for sensitive fluorometric determination of cartap based on its aggregation effect on gold nanoparticles. Microchim Acta 186(4):259. https://doi.org/10.1007/s00604-019-3361-5